Array of Microfluidic Beam Resonators for Density and Viscosity Analysis of Liquids

S. Marquez, M. Alvarez, D. Fariña, A Homs-Corbera, C. Dominguez and L.M Lechuga *Member, IEEE*

***Abstract*—This paper reports on the design, fabrication and evaluation of a mass density and viscosity sensor based on an array of polysilicon microbeam resonators integrated with 20 pL fluidic microchannels. When filled with water, resonators exhibit resonant frequencies close to 500 KHz and Q-factor values of 400 operating at atmospheric pressure and ambient temperature. Real-time measurements are highly reproducible and only require 250 µL of the sample fluid. The built-in interferometric readout enables automatic detection of the beams, increasing the throughput analysis and reducing detection times. The frequency shift response shows a linear behavior in accordance with the density of evaluated solvents, organic solutions and alcoholic drinks, reporting a mass responsivity of 7.4 Hz/pg. Also, the sensor is capable of measuring the viscosity of liquid phase samples with a resolution of 0.15 cP by tracking the Q-factor response of the sensor within a linear regime between 1 cP to 2.6 cP. This approach demonstrates the ability to identify in real-time changes of fluids in the liquid phase that could provide a valuable assessment for bioanalytical applications.**

***Index Terms*—Array, density, liquids, microfluidic channels, Q-factor, resonators, resonant frequency, viscosity.**

I. INTRODUCTION

IDENTIFICATION of changes in fluid properties of samples is essential for a wide range of industrial and medical applications. Density and rheological properties of fluids, such as viscosity, are employed to detect food quality [1]-[2], DNA solutions [3] and even single cells [4]. However, current analytical methods generally require large volume samples, need long evaluation times and have a limited sensitivity range [5],[6]. Over the last decade, microelectromechanical sensors (MEMS) have become one of the most promising tools for the achievement of high sensitive sensors due to their miniature size, low mass, and compatibility with CMOS (complementary metal-oxide semiconductor) technologies [7],[8]. The scope of demonstrated applications of MEMS devices for density and rheological parameters of fluids includes: viscoelastic properties of blood and plasma coagulation [10],[11], viscosity measurements of hydrocarbons, silicone oils, oil/fuel mixtures [11]–[13] and gases [14], characterization of polymer solutions [15], concentration of sugar mixtures [16] and ethanol solutions [1],[17], among others. However, when a MEMS resonator is immersed in a viscous fluid, the overdamped response of the resonator produces a rapid dissipation of energy degrading the sensitivity of the sensor with respect to the viscosity of the medium.

An innovative approach to solve this limitation was proposed by Burg et al. [18]. This approach involved integrating a fluidic channel into a suspended microcantilever, namely suspended microchannel resonator (SMR), thereby avoiding damping and viscous drag produced by the fluid environment. Since then, various solutions have been proposed to improve the sensitivity of SMR devices either by decreasing their effective mass or by proposing different materials and designs on their geometry. For example, Khan et. al [13] used silicon-rich nitride (SRN) as structural material to build transparent microchannels that facilitated the visual inspection of processes taking place inside the channels. This approach further derived density and viscosity measurements in liquid phase reagents. Suspended resonators have also been fabricated based on embedded microchannels in plate Lamé resonators to exhibit higher frequency responses and Q-factor values without the need for vacuum and packaging [19]. Another solution reported the fabrication of a suspended doubly clamped beam sensor at nanoscale dimensions with the aim of reducing the effective mass of the resonator [20]. Despite these promising advantages, reducing the mass and size of resonators in order to achieve sensitive transducers complicates the fabrication process. Furthermore, kinetics plays an important role in these type of devices due to the maximum volume of fluid that can flow through the microchannels and the maximum achievable flow rates to optimize the detection times [21]. Whereas a single SMR device is highly sensitive and suitable for identifying individual reagents, a device approach that includes

Manuscript received December 23, 2016. This work was supported in part by the National Council for Science and Technology (CONACyT-Mexico) and the ICTS IMB-CNM (CSIC) clean-room facilities under project NGG-244. The nanoB2A is a consolidated research group (Grup de Recerca) of the Generalitat de Catalunya and has support from the Departament d'Universitats, Recerca i Societat de la Informació de la Generalitat de Catalunya (2014 SGR 624). ICN2 is the recipient of Grant SEV-2013-0295 from the "Severo Ochoa Centers of Excellence" Program of Spanish MINECO.

S. Marquez, D. Fariña, A Homs-Corbera and L.M Lechuga are with Nanobiosensors and Bioanalytical Applications Group, Catalan Institute of Nanoscience and Nanotechnology (ICN2) CSIC, The Barcelona Institute of Science and Technology, Campus UAB, Bellaterra, 08193 Barcelona, Spain and with the CIBER-BBN Networking Center on Bioengineering, Biomaterials and Nanomedicine, Spain (e-mail: salomon.marquez@icn2.cat; dfarinas@cin2.es; antoni.homs@icn.cat; laura.lechuga@icn2.cat)

M. Alvarez and C. Dominguez are with the Microelectronics Institute of Barcelona (IMB-CNM), CSIC, Barcelona, Spain (e-mail: mar.alvarez@imb-cnm.csic.es; Carlos.Dominguez@imb-cnm.csic.es)

This paper has supplementary downloadable material that consists of a video.

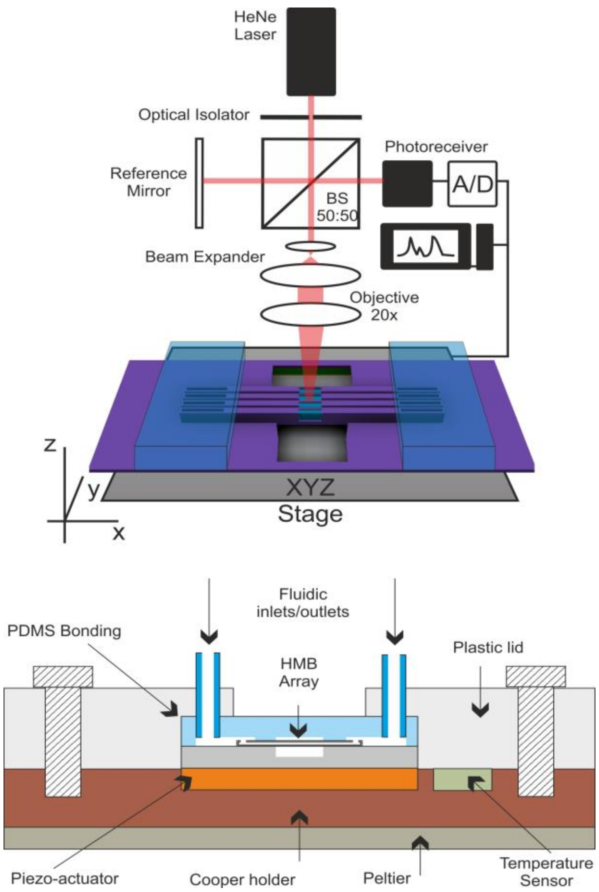

Fig. 1 (*Top)* Schematic view of the HMB sensor and the experimental setup. A custom free space interferometer acquires the driven excitation response of the resonators while a sample solution is streaming through the embedded microchannels. During experiments, temperature was fixed at 23º C ± *0.1*. *(Bottom)* Details of the copper fixture housing the Peltier module and the piezo-ceramic actuator for driving the excitation of the resonators.

an array of resonators with single inlet/outlet embedded microchannels can constitute an efficient sensing platform for reducing sample evaluation times. Besides, this new approach can be used for the simultaneous detection of different samples in real-time.

Therefore, in our approach, we have developed a mass density and viscosity sensor for the real-time identification of Newtonian fluids in the liquid phase using an array of suspended polysilicon microbeams, namely Hollow Microbeam (HMB) resonators (see Fig. 1). The sensor consists of four closely spaced doubly clamped beams with embedded microfluidic channels wherein each microchannel has a volume of around 20 pL. The solution drawn up in our work includes four main contributions: fabrication of a sensor array of resonators with embedded microchannels, implementation of an experimental readout for automatic detection, increase of the precision of rheological measurements of liquids, and usage of polysilicon as main structural material of the sensor. As proof of concept, we have studied the sensor performance in a flow-through detection mode to measure density and viscosity of different solvents and organic solutions. Also, we have analyzed commercial alcoholic beverages demonstrating that the HMB resonators can reduce to 7 min the time employed to measure and validate both the density and viscosity of liquids (17 min) using conventional sensors such as pycnometers and U-tube viscometers.

II. Principle of Operation

For the operation of the HMB sensor, we evaluated the shift in the resonant frequency of the resonator due to changes in its effective mass when a sample fluid of specific density is streaming through the embedded microchannel. The frequency behavior of a doubly clamped beam with an embedded microchannel is modeled as a lump-parameter resonator according to the Euler-Bernoulli beam theory [28]. The model is valid under the following assumptions: 1) the material composition of the resonators is uniformly distributed along the length of the structures and the cross-section geometry of the microchannels is constant, 2) the fluid filling of embedded microchannels does not change the elastic constant of the resonators and, 3) shearing deformation of the doubly clamped beams is negligible. For low-damping values, the resonant frequency of a resonator (ω_r) can be approximated to its natural frequency (ω_0), as $\omega_r \approx \omega_0$. Then, the resonant frequency of a linear resonator with elastic constant (k_b) and effective mass (m_b) is:

$$\omega_r^2 = \frac{k_b}{m_b} \tag{1}$$

Here, the elastic constant is defined as $k_b = 192EI/L^3$ where *E* is the Young Modulus, *I* is the moment of inertia of the empty beam with respect to y-axis and *L* is the beam length, respectively. The moment of inertia is defined as $I = (w_b h_b^3 - w_f h_f^3)/12$ being w_f and h_f, the width and height of the embedded microchannel, and w_b and h_b, the width and height of the beam, respectively. The total effective mass of the resonator is a contribution of not only the structural material but also of the added mass induced by the sample fluid. For this reason, we modeled the resonators as a multimorph doubly clamped beams formed by equal length layers in which the effective mass is defined as [23]:

$$m_b = \frac{26}{70} L \sum_{i=1}^{n} \rho_i A_i \tag{2}$$

where ρ_i is the density of the layer "i" with its corresponding cross-sectional area A_i. By substituting the lump-parameter definitions of k_b and m_b into (1), the approximated fundamental resonant frequency of the HMB resonator is:

$$f_{r,b} = \frac{22.736\, h_b}{2\pi L^2} \sqrt{\frac{E}{12[\alpha\rho_f + (1-\alpha)\rho_b]}} \tag{3}$$

where ρ_b and ρ_f are the structural material and sample fluid densities, respectively. The parameter α is the ratio of the microfluidic channel surface to the beam cross-sectional area defined as $\alpha = w_f h_f / w_b h_b$. By monitoring the HMB resonant frequency response, we correlated the frequency changes as a function of the sample fluid density.

The quality factor (Q) defines the ratio of stored energy to the dissipated energy on each oscillation cycle of a resonator. On SMR devices, the dissipation of energy is mainly attributed to shearing of the contained fluid that is able to freely move inside the channel. Besides, as damping is a non-monotonic function of the sample viscosity inside of SMR resonators [24], the Q-factor value can increase or decrease with respect to sample viscosity [25]. Since the embedded microchannel is centered about the beam neutral axis in our approach, the magnitude of the shearing effect can be determined by the dimensionless frequency number $\beta = \rho_{fluid}\omega h^2_{fluid}/\mu$, where h_{fluid} is the channel height, μ is the dynamic viscosity, ρ_{fluid} is the fluid density and ω is the resonant frequency, respectively. Sader et al. [25] derived a non-monotonic function $F(\beta)$ to understand the effect of the energy dissipation of SMR devices as a function of the β number. For the fundamental frequency mode of resonators, the non-monotonic function $F(\beta) \approx 0.152\sqrt{\beta} + 38.7/\beta$ [24] defines two flow transition regimes at its minimum (β=46). For β<46, there is a low-inertia regime whereas for β>46, fluid inertia dominates. The dimensionless function $F(\beta)$ yields a maximum error estimation of 13% for all β. According to the fabricated dimensions of our resonators and the used liquid samples, low-inertia regime dominates in the HMB devices. By tracking the quality factor of the resonators while streaming different liquid samples, we analyzed the sensor response to viscosity changes.

Another important design parameter of the HMB resonators is related to the limits of pressure at both ends of the microchannel inlets in order to avoid the collapsing of the inner channel walls. A reasonable approximation with less than 10% error, for aspect ratios of h/w ≤ 0.7, introduces a pressure difference of [26]:

$$\Delta P\left[1-\frac{6(2^5)}{\pi^5}\frac{h_f}{w_f}\right]=\frac{12\mu L}{wh_f^3}Q_{flow} \tag{4}$$

where ΔP is the pressure difference along the microfluidic channel; μ is the water viscosity (1 cP) and Q_{flow} defines the flow rate (μL/min), respectively. According to this relationship, we can theoretically inject solutions at a pressure difference of up to 7 MPa, yielding flow rates of up to 45 μl/min.

III. FABRICATION AND CHARACTERIZATION

A. Device Design and Fabrication

Four embedded microfluidic channels of 1300 μm in length and cross-sectional area of 20 μm x 4 μm integrate the array of nominally identical resonators, with a distance between each other of 13 μm, as Fig. 2 shows. This design establishes very short separation distances between the hollow doubly clamped beams so that the response of the sensors can be acquired by the optical readout system. The microchannel wall thickness is 1 μm. The effective length of each resonator (about 275 μm) is set at each clamped side of a rectangular trench of 275 μm x 7500 μm. Fluidic inlets of 10 μm x 100 μm in dimension are located at both end sides of the microchannels. To allow fluid exchange inside of the embedded microchannels, two polydimethylsiloxane (PDMS) delivery channels of cross-sectional area of 200 μm x 35 μm and length of 1.5 mm are integrated on both sides of the inlets of HMB resonators. The serpentine design of the PDMS fluid delivery channels is done in order to facilitate the visual inspection of the meniscus of the liquids during the filling step of the HMB sensors.

Hollow microbridges were fabricated using 4-in, type p silicon wafers of 500 μm thickness. Polysilicon was used as structural layer and boron phosphorus doped silicon oxide (BPSG) as sacrificial layer because of its high selectivity to polysilicon and high etching rate with HF 49%. Thereafter, a 1 μm layer of polysilicon was deposited by low-pressure chemical vapor deposition (LPCVD) at 580ºC and 380 mtorr. The 4 μm topology of microfluidic channels was patterned by reactive ion etching and hard contact photolithography. As follows, another layer of 1 μm polysilicon was coated in order to enclose the microchannels. Access holes, located at both ends of the structures were etched on top of the polysilicon layer in order to

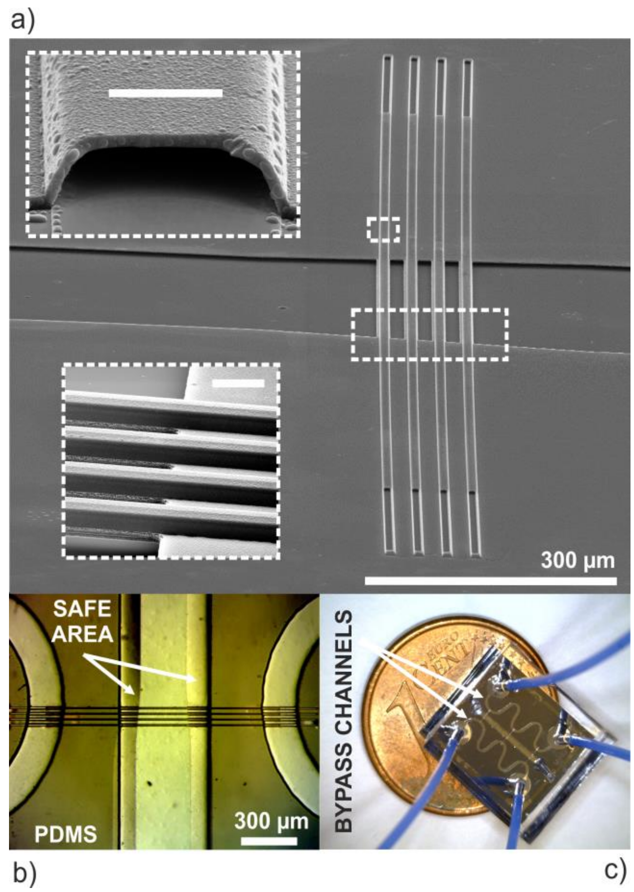

Fig. 2 a) Scanning electron microscope image of an array of four HMB resonators; inset 1 shows the cross section of an embedded microchannel of 20 μm x 4 μm with 1 μm thick polysilicon structural layer; inset 2 illustrates the 4 μm topology and lateral distance of 13 μm between the suspended array of resonators. Scale bar represents 10 μm. b) Optical microscope image illustrating the PDMS bypass channels connecting with the inlets of the HMB resonators. A safe area was set along the edges of the sensors (50 μm) to avoid any leakage of uncured PDMS onto the structures. c) Chip with integrated microfluidics and external tubing connections for injection of sample solutions (dimensions 1 cm x 1 cm).

dissolve the sacrificial layer. Also, in this step, the length of the resonators was defined. Using HF 49%, up to 1300 μm long channels were emptied after approximately 25 min of isotropic wet etching. The resonators were released in this procedure by dissolving the SiO_2 PECVD TEOS 2:1 beneath the polysilicon microbeams at a lower etching rate than the BPSG sacrificial layer. Finally, the wafer was manually diced to have chips of 1 cm x 1 cm. A scanning electron image of the final array of doubly clamped beams is illustrated in Fig. 2a. Further details of device fabrication are described in [27].

For injection of liquids inside the array of resonators, PDMS bypass channels were replicated from a master mold of SU-8 negative photoresist (Microchem SU-8 2025). The master mold was fabricated by standard photolithography [28]. First, the photoresist was spun onto a silicon substrate to obtain a 35 μm thick layer and by soft-photolithography, the bypass channels were patterned. The 4 mm thick PDMS replica was prepared by a 10:1 ratio of elastomer and curing agent from "Sylgard 184 Silicon elastomer Kit". PDMS was cured in a hot plate at 80º C for 2 hrs. Thereafter, four through holes were perforated on each PDMS reservoir of the bypass channels with a biopsy punch (Harris Uni-CoreTM 1 mm I.D.) for external access of tubing connections and using a razor blade the PDMS was cut to have dimensions of 1 cm x 1 cm. Permanent bonding of PDMS to the devices was done by a stamp-and-stick technique in which uncured PDMS of 10:3 ratio was used as an adhesive [29]. Applying soft pressure to make the bonding process faster resulted in reflow of the uncured polymer. Also, any increase in temperature caused clogging of the microchannels. Once the uncured PDMS covered all over the surface, except those areas corresponding to the microfluidic channels and the array of resonators, the 10:3 PDMS was let to cure for 48 h at room temperature. This methodology yielded a good sealing of the topology of the structures and prevented any structural damage to the resonators as shown in Fig. 2b. The maximum pressure that this permanent union can withstand is up to 38 psi, which is adequate for flow rates below 100 μl/min. Finally, four PEEK tubes (Valco Instruments Co. Inc. JR-T-6009) of 250 μm of i.d. were affixed to each delivery channel reservoir. Fig. 2b illustrates the chip device with the integrated bypass channels.

B. *Experimental set-up*

Measurement of the HMB resonators was performed by a custom designed optical free-space interferometer. S1 from supporting information shows a detailed scheme of our homebuilt experimental setup. A 632.8 nm HeNe laser beam of 1 mm diameter (JDSU 1101, 1.5mW) passes through an optical isolator (Thorlabs IO-3D-633-VLP) to cancel undesired back-reflections and noise fluctuations. A 50:50 beamsplitter (Thorlabs CM1-BS1) splits the laser beam by half to form a reference path, which reflects back from a reference mirror onto a high-bandwidth photoreceiver (New Focus 1801). On the active arm of the interferometer, the beam is expanded five times with a beam expander (Thorlabs BE05M-A) for imaging purposes and for reducing the final spot size. The laser beam is focused tightly through a 20x microscope objective (Olympus 20x, NA = 0.4) onto the middle point of the structures with the optical axis parallel to the bending motion of the resonators. The spot size of 1.3 μm is calculated according to the Rayleigh criteria: $\omega_0 = 1.64\lambda/2NA$. Finally, the photoreceiver collects the interference pattern of the reflected light from a beam and the light from the reference mirror. All optical components of the experimental setup are rigidly assembled to an optical table with active mechanical isolation to compensate for undesired vibration drifts.

The actuation scheme of the array of resonators was done through a frequency sweep methodology that allowed a fast and high-throughput excitation over a range of frequencies around the central peak response of the resonators [30]. The excitation was achieved by means of a piezoceramic actuator (PImicos PIC181) placed beneath the chip, as Fig. 1 shows. The driven response of the resonators was acquired by a synchronization protocol between a function generator (Agilent 33220A) and a fast acquisition card (National Instruments PXI-5922) that avoided cross-talk interference between actuated and acquired signals. The function generator controlled the amplitude (1.5 Vpp) and sweep time (100 ms) of a sine-wave excitation signal over a 200 KHz bandwidth around the central peak response of the resonators. Sequential evaluation of every resonator response was performed by the optical readout by transversally scanning each of the middle points of the beam resonators under the laser spot using an automated computer controlled 3-axis stage. Finally, we computed the Fast Fourier transform (FFT) of the acquired signals in LabVIEW to obtain the frequency spectrum response. The FFT was averaged three times to reduce noise fluctuations and a Lorentzian curve fitting algorithm computed in real-time the peak frequency response and Q-factor values.

The filling of embedded microchannels was done through an H-shaped microfluidic configuration as Fig. 2b shows. In each measurement, 250 μL of sample volume was loaded and delivered into one of the bypass channels by a low-pressure valve (Valco Instruments Co. Inc. C22-3186) at a constant flow rate of 10 μL/min using a syringe pump (New Era Pump Systems Inc. NE-300). On the other bypass channel, a constant flow rate of 1 μL/min rinsed the output of the microchannels continuously.

The calibration protocol of our sensor consisted of measuring the response of the resonators filled with air and water before determining the density and viscosity of samples. The response of the HMB devices was automatically captured by the optical readout interferometer while the resonators were actuated through the sweep frequency methodology. The temperature of the sensor was stabilized at 23º C by a closed loop temperature controller (Thorlabs T-Cube TEC Controller) with a resolution of 0.1º C. Measurements were taken after 5 min of sample injection to ensure the liquid exchange inside the resonators and temperature stabilization. Then, the resonance frequency and the Q-factor were extracted from the resonance peak for each resonator. A calibration fit was done for the measurements of water and air. Before measuring a new sample fluid, the HMB resonators were cleaned with sodium dodecyl sulfate (SDS), hydrochloric acid 0.1 M (HCl) and rinsed with plenty of water to reduce systematic instabilities on frequency. All measurements were done at least in triplicates.

IV. Results and Discussion

By considering polysilicon as structural material with density of 2331 kg/m^3 and Young Modulus of 160 GPa [31], calculations from (3) showed that the expected fundamental resonant frequency of resonators (L ≈ 275 μm) was approximately 918 KHz when filled with air. Instead, resonators showed a resonance frequency close to 650 KHz ± 10 Hz operating at 23°C and at atmospheric pressure conditions. This frequency variation was attributed to a modification of the effective length of the structures while releasing them from the substrate with the treatment of HF 49% acid during the fabrication process. By an optical characterization with microscope images, we measured a lateral over-etching distance of approximately 25 μm, which modified the final effective length of each beam. Based on calculations from (3), the resonant frequency of resonators with an over-length of 25 μm at each clamped side was approximately of 651 KHz when filled with air. An additional photolithographic mask to empty and release the resonators in two consecutive steps can further reduce the lateral over-etching effect.

After characterizing the resonators in the unfilled state, we studied the performance of the sensors when filled with water. The array of beams exhibited a frequency response close to 502 KHz ± 11Hz, which represents a frequency shift of 148 kHz (22.77%) with respect to their response in air. In the Electronic Supplementary Information (ESI) we show a video of the fluid exchange inside the HMB device. The filling capabilities of the embedded microchannels were successfully proven owing to the physical properties of the internal sidewalls, which presented low porosity and a high planarization level. The frequency shift of the resonators was in accordance with the change in density of the fluid contained inside the microfluidic channels. Sensor noise was estimated based on the evaluation of the standard deviation of the frequency response of the resonators when filled with water, specifically when no frequency variation was expected ($\Delta f_R = 0$). Over a period of 45 min, the resonant frequency peak showed a standard deviation of $\sigma_R = \pm$ 10 Hz. Although random sources of noise were present in the acquisition system, such as laser amplitude fluctuations and variations of the optical focusing of resonators, other sources of error could potentially be controlled. For example, by increasing the number of acquired samples and by reducing the excitation frequency bandwidth, the systematic errors introduced by the Lorentzian curve fitting of the frequency response were minimized.

Thereafter, to calculate the mass responsivity of the device, we used four samples with different and well-known densities (from Sigma Aldrich): diethyl ether (713.4 kg/m^3), isopropanol (786 kg/m^3), ethanol (789 kg/m^3), and acetic acid (1049 kg/m^3). The latter one was chosen to measure the linear response of the sensor beyond the density of the reference liquid (water). Fig. 3 shows the frequency response depicted by these sample solutions with respect to their reference density values for a single resonator. The results demonstrated a clear relationship between the measured resonant frequency peak shift and the sample solution density, according to the model proposed by (3). To determine the sensitivity of the sensor, a linear curve fitting of data within this range of densities was calculated for each HMB resonator, as Table 1 shows. The mass responsivity was obtained by dividing the sensitivity with respect to the volume of a single embedded microchannel (~20 pL). The results show a better mass responsivity than that achieved by two previous SMR approaches [32],[13]. However, the mass responsivity of HMB resonators is surpassed by that of SMR devices with smaller effective mass [19],[20]. Also, our findings demonstrated that a minimum resolvable density change of 0.068 kg/m^3 was achieved for a frequency resolution of ± 10 Hz.

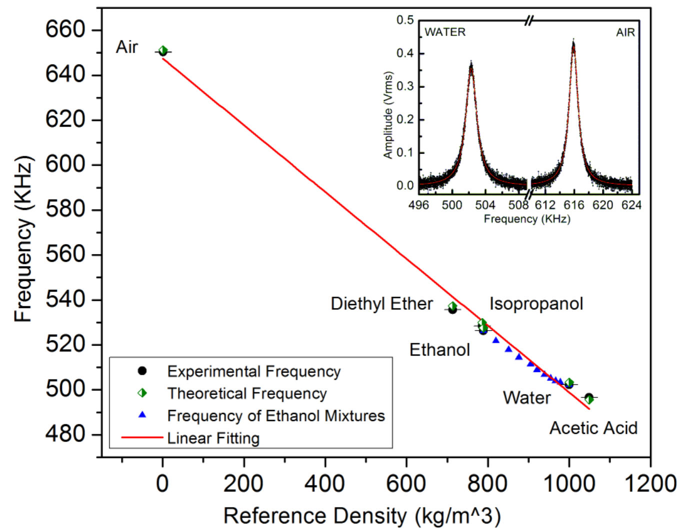

Fig. 3 Resonant frequency response of a resonator when filled with different solutions with well-known densities, including water/ethanol mixtures (blue triangle markers). The inset shows the peak frequency response of the resonator before and after filling it with water indicating a frequency shift of 148 KHz with a 41.1% quality factor decay. Error bars are smaller than black dots and represent a standard deviation of ±10 Hz.

TABLE I
Performances of the Array of HMB Resonators

Bridge	Sensor mass (ng)	Resonance frequency f_0 (kHz) in air	Extracted slope (S_A) Hz/kgm^{-3}	Experimental mass responsivity Hz/pg
B1	17.69	650.119	147.77	7.38
B2	17.30	650.422	147.86	7.39
B3	16.90	651.094	148.19	7.40
B4	16.50	651.262	148.75	7.43

Owing that the mass responsivity of the array of HMB resonators resulted quite similar (~7.4 Hz/pg), the average response of the four sensors was calculated in order to increase the throughput in the analysis of the following samples. To study the sensor performance as a rheology analyzer we prepared binary solutions of ethanol and water. We injected solutions of ethanol with concentrations in volume from 0% to 100%, with increments of 10%. Besides, the density of ethanol/water mixtures was calculated with a commercial pycnometer (10 ml pycnometer, Brand) at a fixed temperature of 23°C to evaluate the frequency response of the sensor as a function of the density of the samples. Fig. 4a shows the average frequency peak measurement over a time period of 10 min for each ethanol concentration. As expected, the interplay between the frequency

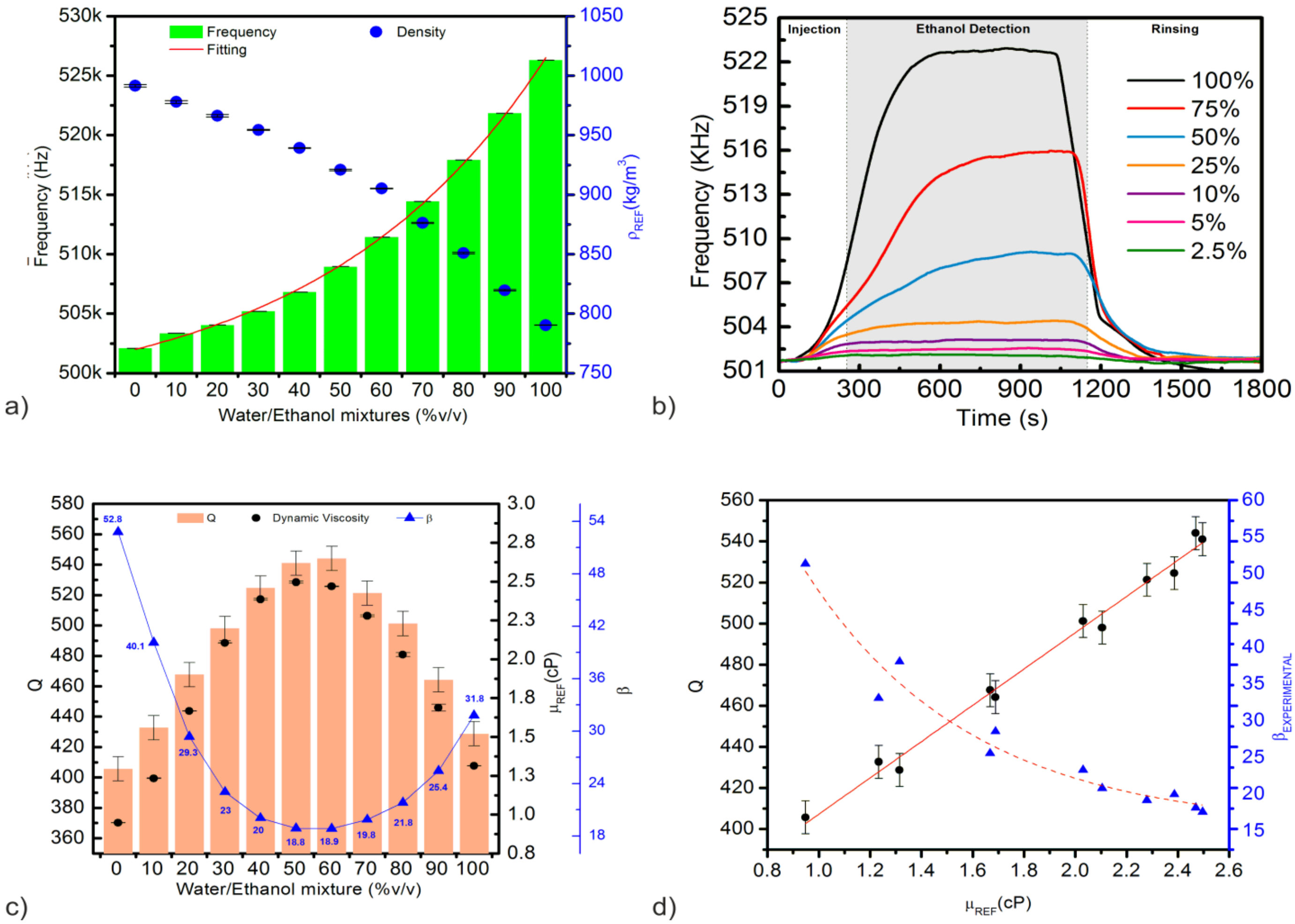

Fig. 4 a) Average resonant frequency response of the HMB resonators with respect to binary mixtures of ethanol and water at different volumetric concentrations ranging from 0% to 100%. Data also shows the inversely proportional interplay of density values measured with a commercial pycnometer. b) Real-time measurements of the shift in the resonant frequency to detect the minimum resolvable %v/v concentration. Dilution effects were noticeable during the first minutes of injection for higher ethanol concentrations. c) A linear tendency is depicted by the Q-factor values as the viscosity of the binary mixtures increases within the viscosity regime from 1 cP to 2.6 cP. d) The experimental values for ß demonstrate de interplay between fluid inertia and Q-factor values.

of the sensor and the density was inversely proportional with respect to the content of water/ethanol mixtures. This tendency was also observed in other calibration protocols [33]. The linear curve fitting of the frequency with respect to the density within this range showed a slope of 146 Hz/kgm^{-3}. As Fig. 4b shows, a complete sample exchange inside of resonators took about 7 minutes for a 10 μL/min flow rate in the inlet bypass channel. We note that this time could be reduced by controlling the inlet bypass channel inflow to diminish dilution effects of mixtures with the initial reference liquid (water) that was contained inside of resonators. Furthermore, the results demonstrated an increasing exponential trend in frequency as the ethanol concentration increased while modifying the sample density according to the following curve fitting equation:

$$f(\%v/v) = 497178.74 + 4824.114\,e^{-0.01806(\%v/v)} \quad (5)$$

From here, the minimum resolvable ethanol concentration of 0.115% was computed for a frequency resolution of $\sigma_R = \pm 10$ Hz. Sensor Signal-to-Noise ratio (SNR) was calculated for the minimum ethanol concentration as $\Delta f_{2.5\%}/\sigma_R$; where $\Delta f_{2.5\%}$=418 Hz is the frequency shift derived from a 2.5% ethanol concentration, as shown in Fig. 4b, yielding a SNR of 41.8.

As regards the energy dissipation of the HMB device, the reported Q-factor value of resonators was 692±10 in air. However, after filling the microfluidic channels with water, the Q-factor decreased to 405.70±10 for all the resonators, which represents a decay of 41.1%. This effect is similar to another approach of SMR devices [24] when the air was replaced with water showing a 40% decay of the quality factor. To better understand this behavior, we compared the average response of the quality factors of the array of resonators when filled with binary mixtures of water/ethanol, with the corresponding dynamic viscosities. The viscosities were calculated with a commercial Ubbelohde viscometer (UBBEL02UKC, Sigma-Aldrich) at a fixed temperature of 23°C, as Fig. 4c shows. Interestingly, the experimental results showed a decrease in the dissipation of energy of the resonators (enhancement of quality factor) as a function of increasing viscosity. This effect is contrary to the Q-factor response depicted by low-stress silicon nitride SMR devices [13] in which the quality factor decreased as a function of increasing viscosity of water/ethanol mixtures. This can be explained in terms of the dimensionless frequency number β by considering the height of our microfluidic channels (h_{fluid} = 4 μm) and taking into account the values of density and viscosity calculated from the reference sensors. For instance, the value of β after filling the microchannel with ethanol was approximately 31.81. Fig. 4c shows that for our device, the computed values of β for water/ethanol mixtures are within the low inertia regime (β<46). In this regime, since there is little inertia, the fluid follows the solid displacement of the resonator resembling a rigid-body oscillation. This explains the improvement in Q-factor values with increasing viscosity from 1 cP to 2.6 cP. From here, we correlated the Q-factor values of water/ethanol samples with respect to their reference viscosity values as shown in Fig. 4d, which resulted in a empirical linear behavior for the water/ethanol mixtures according to the following curve fitting approximation:

$$Q(\mu) = 325.78 + 82.5(\mu) \qquad (6)$$

The non-monotonic interplay between the water/ethanol samples and the Q-factor, along with the polar nature of the ethanol and water molecules indicate that (6) is applicable within a short range of viscosities. From here, the minimum resolvable viscosity change of 0.15 cP was computed for a Q-factor resolution of ±10. Experimentally, β decreased exponentially as a function of sample viscosity, which confirms the low-inertia regime of the sensor, as Fig. 4d shows.

Finally, we tested the device performance to measure the density and viscosity of a variety of alcoholic beverages. We compared four distilled beverages that contained no added sugar (spirits), and one distilled beverage with added sugar and flavorings. For the group of distilled alcoholic beverages, there was a close correlation as density increased with a percentage error below 0.56%. In particular, beverages such as vodka, whisky and rum, which contain 40% of Alcohol by Volume (ABV), depicted close frequency values among them with an average resonant frequency of 506.6 KHz ± 11 Hz, as Fig. 5a shows. However, measurements with coffee liquor exhibited a frequency response (496.105 KHz ± 11 Hz) below the frequency response of water, showing that sugar concentration and flavorings influence density values more than the ethanol content. In comparison with the time used by U-tube viscometers (~15 min) and pycnometers (~2 min) to determine the viscosity and density of alcoholic drinks, the HMB device significantly reduced the time for calculating both parameters. In a single measurement both the viscosity and density of alcoholic drinks were determined with our methodology in 7 min requiring sample volumes of only 250 μl. Afterwards, we calculated by (6) the dynamic viscosity of the alcoholic drinks by tracking the response of the Q-factor of the sensor (see Fig. 5b). We compared the calculated dynamic viscosity of each alcoholic drink with their corresponding dynamic viscosity obtained using the U-tube sensor. The results showed a percentage error below 2%. Deviations from the

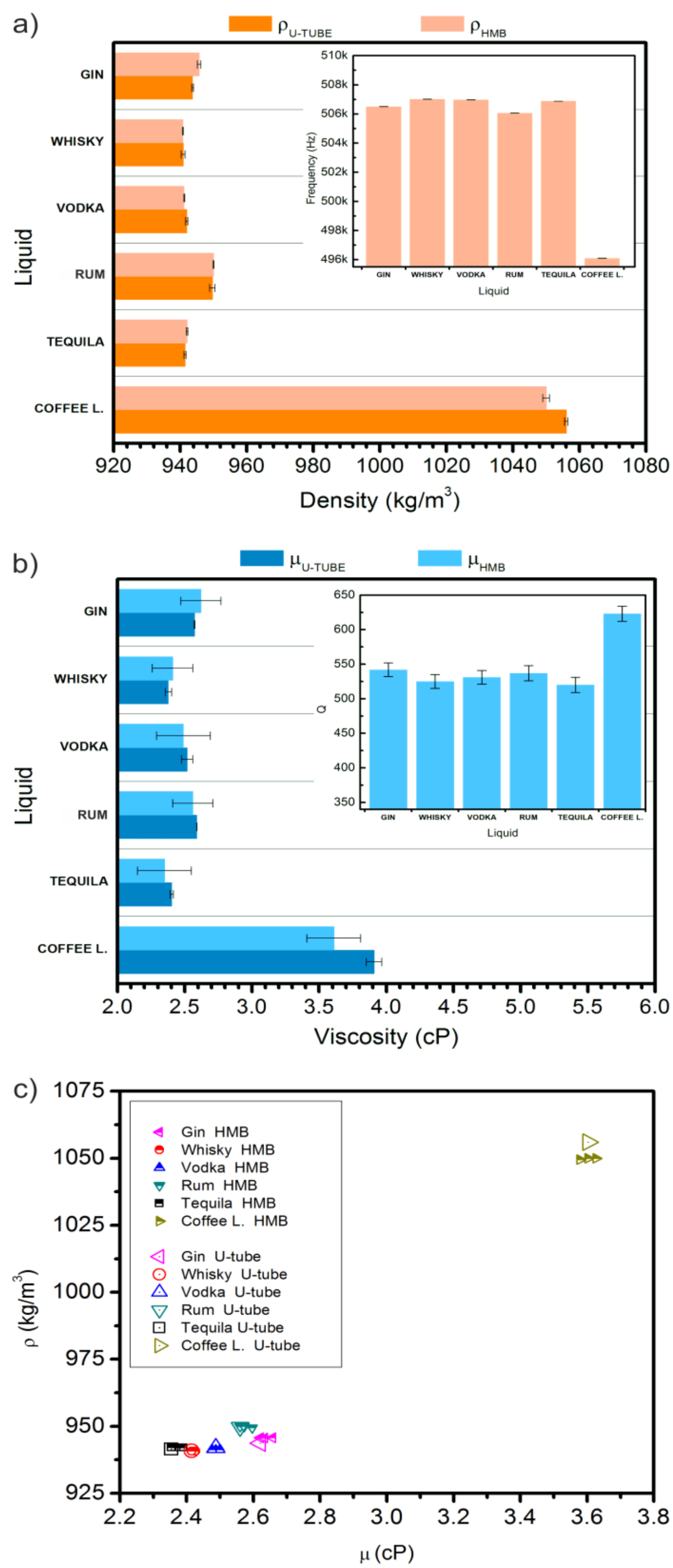

Fig. 5 a) Resonant frequency response of various alcoholic drinks. b) Calculated viscosity of distilled alcoholic drinks (the error increases for viscosities beyond 2.6 cP as is the case for the coffee liquor). c) Comparison of experimental values from the HMB sensor with respect to the values from reference sensors for identification of alcoholic drinks.

expected value (7.67%) were observed for the coffee liquor beverage given that its dynamic viscosity is out of the linear viscosity regime of the HMB sensor. Error bars of the HMB viscosity measurements in Fig. 5b make challenging the identification of individual alcoholic beverages with close ABV percentages. The accuracy of the dynamic viscosity measurements can be improved by operating the sensors in a moderate vacuum environment. Identification of alcoholic drinks with the HMB devices is only feasible as a function of both the obtained density and dynamic viscosity as Fig. 5c shows.

Regarding the material properties of the sensor, a structural material such as polysilicon can be easily oxidized by different methods such as thermal oxidation or by direct streaming of oxidation agents. This advantage is of importance in order to modify the hydrophilic properties of the inner microfluidics walls to facilitate the filling of resonators with fluids of different viscosities. Another advantage of polysilicon is the reduced time for etching the sacrificial layer in only a few minutes.

V. Summary and Conclusions

We have validated the fabrication and performance of an array of polysilicon doubly clamped resonators with embedded microfluidic channels to work as a mass density and viscosity sensor. The fabrication of the devices was accomplished using standard surface micromachining techniques. The doubly clamped configuration of the resonators provided more flexibility for fabricating straight microchannels with different dimensions to facilitate the input and output of liquid phase solutions and also to reduce the clogging of the microfluidic channels.

We have achieved a proper on-chip integration of polymer-based channels using a permanent bonding strategy with PDMS. This included the sealing with good step coverage of microstructures with features that protruded out from the based substrate. On the other hand, the implemented optical readout granted the efficient acquisition of the nanometric out-of-plane displacements of the HMB devices automatically. Enhancing the frequency resolution of the detection system by implementing parametric feedback oscillator methodologies and operating the devices in a moderate vacuum can continuously improve the sensitivity and resolution of HMB devices at least one order of magnitude as it has been demonstrated by a previous approach [34].

The experimental results demonstrated that the system could be used for high-throughput measurement of liquid phase analytes. We have experimentally proven the linearity between the resonance frequency shifts of the resonators and the liquid density, when testing different samples ranging from solvents, organic solutions to alcoholic beverages, streamed through the embedded microchannels in real-time. Furthermore, we found a correlation of the viscosity of the samples as a function of increasing the Q-factor value of the resonators. Due to the non-monotonic energy dissipation of the HMB device, sample viscosity measurements were feasible in a short linear regime, between 1 cP to 2.6 cP, with a resolution of 0.15 cP. Importantly, the array of HMB resonators could characterize low volumes of liquids at atmospheric pressure conditions with a better mass responsivity (7.4 Hz/pg) than current SMR devices [13] and with a comparable response to another competitive approach [32]. Thus, this work is a step towards the development of a multiplexed platform capable of rapid monitoring of rheological properties of distinct fluid samples.

Acknowledgment

Authors acknowledge the support from National Council for Science and Technology (CONACyT-Mexico). We are also thankful to V. Solis-Tinoco for her collaboration and discussions in the microfluidic integration of devices.

References

[1] R. Paxman, J. Stinson, A. Dejardin, R. A. McKendry, and B. W. Hoogenboom, “Using Micromechanical Resonators to Measure Rheological Properties and Alcohol Content of Model Solutions and Commercial Beverages,” *Sensors*, vol. 12, no. 5, pp. 6497–6507, 2012.

[2] J. F. Vélez-Ruiz and G. V. Barbosa-Cánovas, “Rheological properties of concentrated milk as a function of concentration, temperature and storage time,” J. Food Eng., vol. 35, no. 2, pp. 177–190, 1998.

[3] P. Rust, D. Cereghetti, and J. Dual, “A micro-liter viscosity and density sensor for the rheological characterization of DNA solutions in the kilo-hertz range,” Lab. Chip, vol. 13, no. 24, pp. 4794–4799, 2013.

[4] M. Godin, A. K. Bryan, T. P. Burg, K. Babcock, and S. R. Manalis, “Measuring the mass, density, and size of particles and cells using a suspended microchannel resonator,” Appl. Phys. Lett., vol. 91, no. 12, pp. 123121-123121–3, 2007.

[5] J. Zhang, C. Dai, X. Su, and S. J. O’Shea, “Determination of liquid density with a low frequency mechanical sensor based on quartz tuning fork,” Sens. Actuators B Chem., vol. 84, no. 2–3, pp. 123–128, 2002.

[6] P. Enoksson, G. Stemme, and E. Stemme, “Fluid density sensor based on resonance vibration,” Sens. Actuators Phys., vol. 47, no. 1–3, pp. 327–331, 1995.

[7] I. Etchart et al., “MEMS sensors for density–viscosity sensing in a low-flow microfluidic environment,” Sens. Actuators Phys., vol. 141, no. 2, pp. 266–275, 2008.

[8] B. A. Bircher et al., “Real-Time Viscosity and Mass Density Sensors Requiring Microliter Sample Volume Based on Nanomechanical Resonators,” Anal. Chem., vol. 85, no. 18, pp. 8676–8683, 2013.

[9] L. Müller et al., “Investigation of Prothrombin Time in Human Whole-Blood Samples with a Quartz Crystal Biosensor,” Anal. Chem., vol. 82, no. 2, pp. 658–663, 2010.

[10] O. Cakmak et al., “Microcantilever based disposable viscosity sensor for serum and blood plasma measurements,” Methods, vol. 63, no. 3, pp. 225–232, 2013.

[11] M. Youssry, N. Belmiloud, B. Caillard, C. Ayela, C. Pellet, and I. Dufour, “A straightforward determination of fluid viscosity and density using microcantilevers: From experimental data to analytical expressions,” Sens. Actuators Phys., vol. 172, no. 1, pp. 40–46, 2011.

[12] J. Toledo et al., “Comparison of quartz tuning forks and AlN-based extensional microresonators for viscosity measurements in oil/fuel mixtures,” in Proc. SPIE 8763, Smart Sensors, Actuators, and MEMS VI, 2013, p. 87630L.

[13] M. F. Khan et al., “Online measurement of mass density and viscosity of pL fluid samples with suspended microchannel resonator,” Sens. Actuators B Chem., vol. 185, pp. 456–461, 2013.

[14] S. Boskovic, J. W. M. Chon, P. Mulvaney, and J. E. Sader, “Rheological measurements using microcantilevers,” J. Rheol. 1978-Present, vol. 46, no. 4, pp. 891–899, 2002.

[15] N. McLoughlin, S. L. Lee, and G. Hähner, “Temperature dependence of viscosity and density of viscous liquids determined from thermal noise spectra of uncalibrated atomic force microscope cantilevers,” Lab. Chip, vol. 7, no. 8, p. 1057, 2007.

[16] M. Hennemeyer, S. Burghardt, and R. W. Stark, “Cantilever Micro-rheometer for the Characterization of Sugar Solutions,” Sensors, vol. 8,

no. 1, pp. 10–22, 2008.
[17] N. McLoughlin, S. L. Lee, and G. Hähner, "Simultaneous determination of density and viscosity of liquids based on resonance curves of uncalibrated microcantilevers," Appl. Phys. Lett., vol. 89, no. 18, p. 184106, 2006.
[18] T. P. Burg et al., "Vacuum-Packaged Suspended Microchannel Resonant Mass Sensor for Biomolecular Detection," J. Microelectromechanical Syst., vol. 15, no. 6, pp. 1466–1476, 2006.
[19] V. Agache, G. Blanco-Gomez, F. Baleras, and P. Caillat, "An embedded microchannel in a MEMS plate resonator for ultrasensitive mass sensing in liquid," Lab. Chip, vol. 11, no. 15, pp. 2598–2603, 2011.
[20] R. A. Barton, B. Ilic, S. S. Verbridge, B. R. Cipriany, J. M. Parpia, and H. G. Craighead, "Fabrication of a Nanomechanical Mass Sensor Containing a Nanofluidic Channel," Nano Lett, vol. 10, no. 6, pp. 2058–2063, 2010.
[21] J. L. Arlett and M. L. Roukes, "Ultimate and practical limits of fluid-based mass detection with suspended microchannel resonators," J. Appl. Phys., vol. 108, no. 8, pp. 84701-84701–11, 2010.
[22] S. M. Han, H. Benaroya, and T. Wei, "Dynamics of Transversely Vibrating Beams Using Four Engineering Theories," J. Sound Vib., vol. 225, no. 5, pp. 935–988, 1999.
[23] N. Lobontiu, Mechanical Design of Microresonators: Modeling and Applications, 1 edition. New York: McGraw-Hill Professional, 2005.
[24] T. P. Burg, J. E. Sader, and S. R. Manalis, "Nonmonotonic Energy Dissipation in Microfluidic Resonators," Phys. Rev. Lett., vol. 102, no. 22, p. 228103, 2009.
[25] J. E. Sader, T. P. Burg, and S. R. Manalis, "Energy Dissipation in Microfluidic Beam Resonators," J. Fluid Mech., vol. 650, pp. 215–250, 2010.
[26] A. Folch, Introduction to BioMEMS. CRC Press, 2012.
[27] S. Marquez, M. Alvarez, D. Farina, C. Dominguez, and L. M. Lechuga, "Towards a biosensing multiple platform based on an array of hollow microbridge resonators," in 2014 IEEE SENSORS, 2014, pp. 329–331.
[28] D. Qin, Y. Xia, and G. M. Whitesides, "Rapid prototyping of complex structures with feature sizes larger than 20 µm," Adv. Mater., vol. 8, no. 11, pp. 917–919, 1996.
[29] R. W. R. L. Gajasinghe et al., "Experimental study of PDMS bonding to various substrates for monolithic microfluidic applications," J. Micromechanics Microengineering, vol. 24, no. 7, p. 75010, 2014.
[30] C. I. Enriquez-Flores, J. J. Gervacio-Arciniega, E. Cruz-Valeriano, P. de Urquijo-Ventura, B. J. Gutierrez-Salazar, and F. J. Espinoza-Beltran, "Fast frequency sweeping in resonance-tracking SPM for high-resolution AFAM and PFM imaging," Nanotechnology, vol. 23, no. 49, p. 495705, 2012.
[31] S. D. Senturia, Microsystem Design. Springer US, 2005.
[32] J. Lee et al., "Suspended microchannel resonators with piezoresistive sensors," Lab Chip, vol. 11, no. 4, pp. 645–651, 2010.
[33] I. S. Khattab, F. Bandarkar, M. A. A. Fakhree, and A. Jouyban, "Density, viscosity, and surface tension of water+ethanol mixtures from 293 to 323K," Korean J. Chem. Eng., vol. 29, no. 6, pp. 812–817, 2012.
[34] S. Olcum et al., "Weighing nanoparticles in solution at the attogram scale," Proc. Natl. Acad. Sci., p. 201318602, 2014.

Salomón Marquez received his MSc degree in Electrical Engineering from The Center for Research and Advanced Studies of the National Polytechnic Institute (CINVESTAV-Mexico) back in 2010. In 2016, he obtained his Ph.D. in electronics engineering working at the Catalan Institute of Nanoscience and Nanotechnology (ICN2, CSIC) in the Nanobiosensors and Bioanalytical Applications group developing MEMs/NEMs technology with embedded microchannels for biosensing applications. His fields of interest include design and modeling of MEMs devices, integration of microfluidic applications and development of biomedical sensors.

Mar Álvarez is currently a researcher at the Biomedical Applications Group at the Institute of Microelectronics of Barcelona of the Spanish National Research Council (IMB-CNM, CSIC). Her main research interest is focused on the technological development of microfluidics and biosensor devices and its integration on lab-on-a-chip and organ-on-chip platforms for the performance of a wide range of biomedical applications. She obtained her MSc and PhD degrees in Physics from the Autonoma University of Madrid, Spain.

David Fariña Santana is a researcher at the Nanobiosensors and Bioanalytical Applications group and the Catalan Institute of Nanoscience and Nanotechnology (ICN2), with a special interest in software and hardware development for optical biosensors and their integration in lab-on-chip platforms. He obtained the ME degree and the PhD in Telecommunications Engineering at the University of Las Palmas de Gran Canaria, Spain.

Antoni Homs-Corbera is, since March 2015, a researcher at the Catalan Institute of Nanoscience and Nanotechnology (ICN2). He graduated from the Universitat Politècnica de Catalunya (UPC, ES) in Telecommunications and Electronics Engineering, back in 1999. Later, he received the degrees of Master in Biomedicine, from the Universitat de Barcelona (UB, Barcelona, ES), and Master in Nanomaterials, from the Imperial College (London, UK). He was awarded his

PhD in Biomedical Engineering from the UPC in 2005. He also holds an MBA for international executives (GEMBA) by IESE since 2013. During his career, he has worked in both private industry and public research, holding positions in several institutions across the globe. His research mainly focusses on the biomedical use of micro and nanotechnologies, BioMEMS and Lab-on-a-Chip devices.

Carlos Dominguez received the B.S., M.S., and Ph.D. degrees in chemistry from the Universidad Complutense of Madrid, Spain, in 1980, and 1985, respectively. He became a member of the scientific staff at the Instituto de Microelectrónica de Barcelona (IMB-CNM, CSIC) in 1986. Since 1991 he has been a Full Professor. He is involved in materials and process development for new transducers and sensors. Currently, he is working on the development of an integrated optical technology based on silicon for (bio)-chemical sensors and broad-band telecommunications applications.

Laura M. Lechuga is Full Professor at the Catalan Institute of Nanoscience and Nanotechnology (ICN2), Spanish National Research Council (CSIC) & CIBER-BBN. Since 2013 she is a Distinguished Visiting professor (PVE) at the Dept. of Microwaves and Photonics, School of Electrical and Computer Sciences, University of Campinas (Brazil) and Fellow of the Optical Society (OSA) since 2014. The principal focus of her research program is the technological development of photonic (plasmonics and silicon-based) biosensors, their integration in portable lab-on-a-chip platforms and their application for clinical and environmental diagnostics. She has published over 200 articles, book chapters and proceedings, has 8 families of awarded patents at European, US or international level,and has presented her work in more than 300 invited talks. She was the driving force for the establishment of one spin-off company in 2004 (SENSIA, S.L.) and co-founder of another spin-off in 2010 (BIOD, S.L.). Prof. Laura Lechuga is associate editor of the IEEE Photonics Journal, associate editor of the J. Optics and Laser Technology (Elsevier).